In vivo human retinal imaging by ultrahigh-speed spectral domain optical coherence tomography

Nader Nassif,* Barry Cense,* B. Hyle Park, and Seok H. Yun

Harvard Medical School and Wellman Center for Photomedicine, Massachusetts General Hospital, 50 Blossom Street, BAR 724, Boston, Massachusetts 02114

Teresa C. Chen

Harvard Medical School and Massachusetts Eye and Ear Infirmary, 243 Charles Street, Boston, Massachusetts 02114

Brett E. Bouma, Guillermo J. Tearney, and Johannes F. de Boer

Harvard Medical School and Wellman Center for Photomedicine, Massachusetts General Hospital, 50 Blossom Street, BAR 724, Boston, Massachusetts 02114

Received September 5, 2003

An ultrahigh-speed spectral domain optical coherence tomography (SD-OCT) system is presented that achieves acquisition rates of 29,300 depth profiles/s. The sensitivity of SD-OCT and time domain OCT (TD-OCT) are experimentally compared, demonstrating a 21.7-dB improvement of SD-OCT over TD-OCT. *In vivo* images of the human retina are presented, demonstrating the ability to acquire high-quality structural images with an axial resolution of 6 μm at ultrahigh speed and with an ocular exposure level of less than 600 μW.

OCIS codes: 170.4500, 110.4280, 170.3890, 030.4280.

Optical coherence tomography (OCT) is a highly sensitive interferometric technique that measures light reflected from within tissue.[1] Nearly all systems developed to date are based on time domain OCT (TD-OCT). In this method the length of the reference arm in an interferometer is rapidly scanned over a distance corresponding to the imaging depth range.

In spectral domain OCT (SD-OCT), also known as Fourier domain OCT, no mechanical scanning of the reference arm is required. Instead, the cross-spectral density at the detection arm of the interferometer is measured by means of a spectrometer.[2] Although this technique has been demonstrated for *in vivo* dermal and retinal imaging,[3,4] it has only recently been demonstrated both theoretically and experimentally that a sensitivity improvement of several orders of magnitude could potentially be realized in SD-OCT compared with TD-OCT.[5,6]

In this Letter we describe an ultrahigh-speed SD-OCT system at 840 nm that acquires depth profiles at a rate of 10,000 and 29,300 per second. In Fig. 1 the experimental setup is shown. The interferometer and slit lamp interface are described in Ref. 7. Briefly, the source was a superluminescent diode (Superlum, Moscow, Russia) with a polarized power of 4.6 mW and a FWHM spectral width of 50 nm centered at 840 nm. In the interferometer configuration employed here, an 80/20 fiber splitter was used, such that 20% of the source light was directed to the slit lamp, where the power incident on the eye was limited to 600 μW by the American National Standards Institute (ANSI) maximum permissible exposure.[8] Upon return from the slit lamp, 80% of the light was directed to the detection arm, resulting in improved collection efficiency. To acquire the cross-spectral density in the detection arm, a high-speed spectrometer was constructed. The light emitted from the detection arm fiber tip was collimated by a lens with a focal length of 50 mm. The collimated beam was incident on a 1200-line/mm transmission grating with a diffraction efficiency of 95%. Diffracted light was then focused onto a 2048-element line scan camera (Basler, Ahrensburg, Germany) with a pixel size of 10 μm $\times$ 10 μm by a three-element lens with a focal length of 100 mm. The quantum efficiency η of the spectrometer–detector combination was 28%, which was determined by the ratio of the optical power detected by the line scan camera and the power at the detection arm fiber tip. The spectral range was 150 nm, and the spectral resolution $\delta\lambda$ was 0.075 nm at a center wavelength λ_0 of 840 nm. In SD-OCT the depth range z is inversely

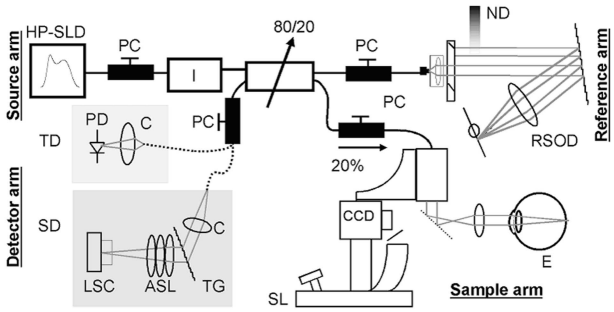

Fig. 1. Schematic of the experimental setup. HP-SLD, source; I, polarizer and isolator; 80/20, fiber-based 80/20 splitter; RSOD, rapid-scanning optical delay line; ND, neutral-density filter; SL, slit-lamp-based telecentric scanner; E, eye; TD, TD-OCT configuration; C, collimator; PD, photodiode; SD, SD-OCT configuration; TG, transmission grating; ASL, three-element air-spaced lens; LSC, line scan camera; PC, polarization controller. For SD-OCT measurements, the RSOD was not scanned and was used for dispersion compensation.

0146-9592/04/050480-03$15.00/0

proportional to the spectral resolution $\delta\lambda$ and is given by[3] $z = \lambda_0^2/4n\delta\lambda$, resulting in a depth range of 2.3 mm in air or 1.7 mm assuming a refractive index of $n = 1.38$ in the eye.

The maximum line rate of the camera was 29.3 kHz and data could be transferred continuously to computer host memory by CameraLink at a resolution of 10 bits/pixel. The maximum digital value (1024) corresponded to 185,000 electrons. Shot-noise-limited detection could be achieved over nearly the full spectrum.

Only the real part of the complex cross-spectral density is detected in SD-OCT, resulting in a signal S_{SD} given by[5,6]

$$S_{\mathrm{SD}} = \frac{\eta^2 e^2 P_{\mathrm{ref}} P_{\mathrm{sample}} {\tau_i}^2}{{E_v}^2}[e^2], \tag{1}$$

where e is the electron charge; P_{ref} and P_{sample} are the reference arm and sample are power per detector element respectively, at the detection arm fiber tip; τ_i is the integration time, and E_v is the photon energy.

The readout and dark noise, shot noise, and relative intensity noise (RIN) contributions to the overall noise in electrons squared per readout cycle and per detector element are given by[5,6]

$${\sigma_{\mathrm{noise}}}^2 = {\sigma_{\mathrm{r+d}}}^2 + \frac{\eta e^2 P_{\mathrm{ref}} \tau_i}{E_v} + \left(\frac{\eta e^2 P_{\mathrm{ref}}}{E_v}\right)^2 \tau_i \tau_{\mathrm{coh}}[e^2], \tag{2}$$

where the sample arm power was assumed to be much smaller than the reference arm power,[9] with ${\sigma_{\mathrm{r+d}}}^2$ being the sum of the readout noise and the dark noise and $\tau_{\mathrm{coh}} = (2\ln 2/\pi)^{1/2}\lambda_0^2/c\delta\lambda$ being the coherence time, where c is the speed of light.[10]

The optimal signal-to-noise ratio (SNR) performance is achieved when shot noise dominates both readout noise and RIN.[9] Shot noise dominates RIN when their ratio is larger than one, i.e., $E_v/\eta P_{\mathrm{ref}}\tau_{\mathrm{coh}} > 1$. With the values for our system, at the detection arm fiber tip, the reference arm power per detector element should be smaller than 40 nW for this condition to be met. Even at the shortest integration time of the camera (34.1 μs), a pixel well will be saturated at a power of 4.6 nW (corresponding to $185,000e$); thus overall system noise will never be dominated by RIN. Based on a measured readout and dark noise of 108 electrons (rms), shot noise dominates readout noise at light levels exceeding 11,664 detected electrons, or 1/16th of the full well depth. The SNR is not limited by the digitization process since the readout and dark noise are larger than half the analog-to-digital resolution ($90e$).

To compare directly the SNR performance of TD-OCT and SD-OCT, a weak reflector was placed in the sample arm of our system. The power reflected by the weak reflector measured at the fiber tip in the detection arm was 1.3 nW. The polarization states of sample and reference are light were carefully aligned to maximize interference. First, 256 depth profiles at a speed of 4 ms per depth profile were acquired with our TD-OCT system, scanning over a depth of 1.4 mm in air. The signal pass bandwidth (BW) was 100 kHz. Then the detection arm was connected to the spectrometer, and 256 spectra were acquired at a speed of 100 μs per spectrum. To reduce fixed pattern noise in the SD-OCT measurement,[5] each individual spectrum was divided by the average spectrum of 1000 reference arm spectra. The resulting spectrum was multipled by a Gaussian to reshape the spectrum.[11] A Fourier transform links z and k space. Because of the nonlinear relation between k and λ, the spectra were interpolated to create evenly spaced samples in the k domain[4] before Fourier transformation of the spectra to generate depth profiles.

Figure 2 shows the averaged depth profiles acquired with the respective configurations, demonstrating a SNR of 44.3 and 50 dB for TD-OCT and SD-OCT, respectively. Both depth profiles were normalized on the reflectivity peak. The TD-OCT measurement was shifted such that the peaks coincide. Some fixed pattern noise was still present in the SD-OCT measurement, resulting in peaks at 84 and 126 μm. Since the SD-OCT system was 5.7 dB more sensitive and operated at a speed 40 times faster (corresponding to 16 dB) than the TD-OCT system, the combined sensitivity improvement was 21.7 dB or a factor of 148. The theoretical shot-noise-limited SNR in TD-OCT and SD-OCT are given by, respectively,[5,6]

$$\mathrm{SNR}_{\mathrm{TD}} = \frac{\eta P_{\mathrm{sample}}}{E_v \mathrm{BW}}, \qquad \mathrm{SNR}_{\mathrm{SD}} = \frac{\eta P_{\mathrm{sample}} \tau_i}{E_v}, \tag{3}$$

resulting in 46.7 dB (TD-OCT) and 51.9 dB (SD-OCT), where $\eta = 0.85$ was used for a photodiode in TD-OCT. The measured TD-OCT and SD-OCT SNRs were respectively 2.4 and 1.9 dB less than the theoretical optimal performance, where 1 dB in TD-OCT was determined to be due to thermal noise contributing to the total noise. The measured coherence function FWHM

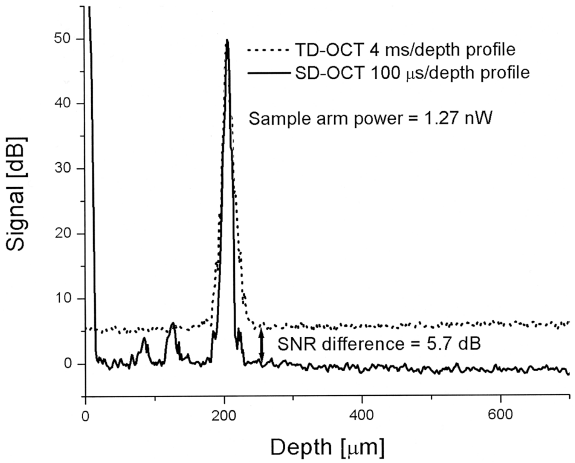

Fig. 2. Comparison of SNR in TD-OCT and SD-OCT for the same weak reflecting surface in the sample arm. Dotted curve, average of 256 depth profiles of the TD-OCT system. Solid curve, average of 256 depth profiles of the SD-OCT system. The large peak at zero in the SD-OCT profile is due to the DC term of the spectrum. The SD-OCT system has a 5.7-dB-higher SNR than the TD-OCT system, at a 40-fold-higher acquisition speed. The depth axis was scaled to reflect ranging assuming a medium with a refractive index of $n = 1.38$.

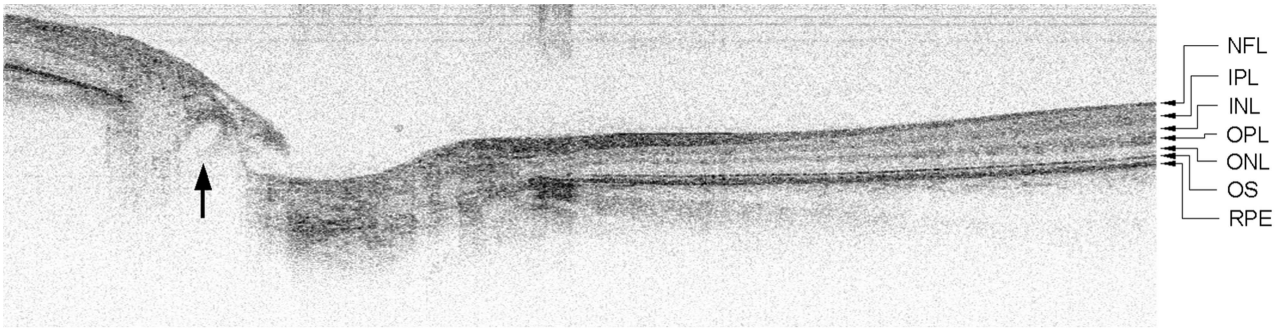

Fig. 3. *In vivo* SD-OCT image of the human retina around the optic nerve head, consisting of 1000 depth profiles acquired in 34 ms. Dimensions are 6.4 mm wide × 1.7 mm deep. Dynamic range within the image was 40 dB. The image shows features that can be identified as[12] the nerve fiber layer (NFL), inner plexiform layer (IPL) inner nuclear layer (INL), outer plexiform layer (OPL), outer nuclear layer (ONL), interface between the inner and outer segments of the photoreceptors (OS), and retinal pigment epithelium (RPE). A blood vessel (indicated with an arrow) can be distinguished near the left side of the optic nerve head.

was 8.3 μm in air, corresponding to 6 μm in tissue ($n = 1.38$). The sensitivity of SD-OCT is expected to drop by 4 dB over the full depth range because of the finite detector element size.[5] Experimentally, a drop of 4 dB was measured over the first one third of the depth range, which might be due to cross talk between adjacent detector elements or a reduced effective spectral resolution.

To demonstrated the ability of our SD-OCT system to acquire high-quality retinal images *in vivo* at ultrahigh speed, the right eye of one human volunteer was measured using an incident power on the cornea of 580 μW. Figure 3 shows an image of an area around the optic nerve head, acquired in 34.1 ms, constructed from 1000 consecutive spectra with an integration time per spectrum of 34.1 μs. To reduce the fixed pattern noise, individual spectra were not corrected with a separately acquired reference spectrum as described earlier but with a spectrum obtained by averaging over the same 1000 spectra of the image. The ratio of the maximum value within the image over the average noise level at a depth of 500 μm was 40 dB. To optimize the display, the image was gray scale coded over a dynamic range of 40 dB, from 4 dB below the maximum value (saturating a small number of data points) to 4 dB below the average noise level at 500 μm. The image shows detailed structures of the optic nerve head and layers of the retina, similar to TD-OCT imaging of the retina.[12] The presence of fixed pattern noise is visible as horizontal lines in the image. In addition, autocorrelation noise, generated by interference of the sample arm light reflected from different depths,[3,4] is visible near the top of the image in depth profiles with strong signals.

In conclusion, we have experimentally demonstrated a sensitivity improvement of SD-OCT over TD-OCT by a factor of 148 (21.7 dB) and ultrahigh-speed *in vivo* human retinal OCT imaging at 29,300 depth profiles/s, resulting in cross-sectional imaging at a video rate with 6-μm resolution. At these speeds, realignment of depth profiles becomes obsolete, revealing the true topography of the optic nerve head. Motion artifacts, commonly present in both research and commercial opthalmic OCT systems are greatly reduced, thus minimizing the image distortion by involuntary eye movement. The demonstrated speed improvement allows for a shift from two-dimensional sampling to comprehensive three-dimensional screening of ocular pathology with OCT.

This research was supported in part by research grants from the National Institutes of Health (1R24 EY12877), the Whitaker Foundation (26083), and the Department of Defense (F4 9620-01-1-0014) as well as a gift from Dr. and Mrs. J. S. Chen to the optical diagnostics program of the Wellman Center for Photomedicine. J. F. de Boer's e-mail address is deboer@helix.mgh.harvard.edu.

*Both authors contributed equally to the work presented.

References

1. D. Huang, E. A. Swanson, C. P. Lin, J. S. Schuman, W. G. Stinson, W. Chang, M. R. Hee, T. Flotte, K. Gregory, C. A. Puliafito, and J. G. Fujimoto, Science **254,** 1178 (1991).
2. A. F. Fercher, C. K. Hitzenberger, G. Kamp, and S. Y. El-Zaiat, Opt. Commun. **117,** 43 (1995).
3. G. Hausler and M. W. Lindner, J. Biomed. Opt. **3,** 21 (1998).
4. M. Wojtkowski, R. Leitgeb, A. Kowalczyk, T. Bajraszewski, and A. F. Fercher, J. Biomed. Opt. **7,** 457 (2002).
5. R. Leitgeb, C. K. Hitzenberger, and A. F. Fercher, Opt. Express **11,** 889 (2003), http://www.opticsexpress.org.
6. J. F. de Boer, B. Cense, B. H. Park, M. C. Pierce, G. J. Tearney, and B. E. Bouma, Opt. Lett. **28,** 2067 (2003).
7. B. Cense, T. C. Chen, B. H. Park, M. C. Pierce, and J. F. de Boer, J. Biomed. Opt. **9,** 121 (2004).
8. American National Standards Institute, *American National Standard for Safe Use of Lasers Z136.1.* (Laser Institute of America, Orlando, Fla., 2000).
9. W. V. Sorin and D. M. Baney, IEEE Photon. Technol. Lett. **4,** 1404 (1992).
10. L. Mandel and E. Wolf, Proc. Phys. Soc. London **80,** 894 (1962).
11. R. Tripathi, N. Nassif, J. S. Nelson, B. H. Park, and J. F. de Boer, Opt. Lett. **27,** 406 (2002).
12. W. Drexler, H. Sattmann, B. Hermann, T. H. Ko, M. Stur, A. Unterhuber, C. Scholda, O. Findl, M. Wirtitsch, J. G. Fujimoto, and A. F. Fercher, Arch. Ophthalmol. **121,** 695 (2003).